Int. J. Heat Mass Transfer. Vol. 29, No. 12, pp. 1843–1853, 1986
Printed in Great Britain

0017–9310/86 $3.00 + 0.00
Pergamon Journals Ltd.

Fully-developed, forced convective flow through an annular packed-sphere bed with wall effects

P. CHENG† and C. T. HSU‡

† Department of Mechanical Engineering, University of Hawaii at Manoa, Honolulu, HI 96822, U.S.A.
‡ Fluid Mechanics Department, TRW Space and Technology Group, Redondo Beach, CA 90278, U.S.A.

(*Received* 27 *November* 1985 *and in final form* 18 *February* 1986)

Abstract—An analysis is performed for a fully-developed, forced convective flow through a packed-sphere bed between concentric cylinders maintained at different temperatures. The radial variations of the porosity and permeability in the bed near the walls, known as wall effects, are approximated by exponential functions. The Brinkman model with variable permeability is used as the momentum equation. An analytical solution based on the method of matched asymptotic expansions is obtained for the velocity distribution. It is shown that velocity overshoots occur in the variable permeability bed near the inner and outer cylinders. Because of the non-uniform porosity variation near the walls, the stagnant thermal conductivity of the bed also varies in the radial direction accordingly. A mixing length theory, proposed recently by Cheng and Vortmeyer for the transverse thermal dispersion, is employed to obtain the radial temperature distribution and the Nusselt number of the annular bed. Computations of the heat transfer characteristics were carried out based on three velocity models, i.e. Brinkman's model with variable and constant permeabilities as well as the plug flow model. It is found that with the mixing length theory, theoretical predictions of the heat transfer characteristics based on the three velocity models are in good agreement with the existing experimental data. The predicted temperature profiles, based on the Brinkman model with a variable permeability, agree the best with temperature data.

INTRODUCTION

THE LUMPED parameter model has often been used to study the performance of a wall-cooled catalytic reactor [1]. The model assumes a plug flow with a constant transverse thermal dispersion coefficient. To account for the higher thermal resistance at the wall, a derivative boundary condition with a finite wall heat transfer coefficient is assumed. The values of the transverse thermal dispersion coefficient and the wall heat transfer coefficient used in the model were obtained experimentally from forced convection in a cylindrical packed column without chemical reactions. The experimental data for the wall heat transfer coefficient is found to be widely scattered [2, 3].

In comparison with experimental data, the lumped parameter model is known to overpredict the hot temperature spots in wall-cooled catalytic reactors [4]. Some investigators [5–7] have attributed this discrepancy to the entrance length effect of the wall heat transfer coefficient and to the plug flow model which does not take into consideration the non-uniform radial velocity distribution; others question [8] the validity that the wall heat transfer coefficient, determined for a packed bed without chemical reactions, can be used for the modeling of the transport process in a catalytic bed.

In a recent paper, Ahmed and Fahien [9] have shown that by allowing the effective thermal conductivity as a function of radius, a wall heat transfer coefficient is not needed to account for the higher thermal resistance at the wall. Most recently, Cheng and Vortmeyer [10] proposed a two-layer mixing length theory for the transverse thermal dispersion process in order to take into consideration the higher thermal resistance at the wall of a packed bed. In their analysis the transverse thermal dispersion coefficient is assumed to be linearly proportional to the Péclet number (Pe); the constants in the mixing length theory as well as in the expression for the transverse thermal dispersion coefficient were determined by matching the predicted temperature profiles and the heat transfer rate to those of experimental data by Schroeder *et al.* [11] for forced convection of water ($Pr = 7.0$) in a rectangular *channel* filled with glass beads at high Reynolds numbers (based on the diameter of the glass beads). With the introduction of the mixing length theory, the large temperature drop near the wall as observed in experiments can be reproduced theoretically; the predicted heat flux is shown to be a function of both the Péclet number as well as the ratio of the particle diameter to the half width of the channel.

In this paper, an analysis is performed for a fully-developed forced convective flow through an *annular* packed bed (see Fig. 1). An analytical solution based on the method of matched asymptotic expansions is obtained for the velocity distribution in the variable permeability packed bed. The two-layer mixing length theory, proposed recently by Cheng and Vortmeyer [10] for the transverse thermal dispersion process is applied to obtain the radial heat transfer charac-

NOMENCLATURE

A	empirical constant defined in equation (2)
B	constant defined in equation (53)
C_1	constant defined in equation (1)
C_2	constant in equation (3)
d_p	particle diameter
D	constant given by equation (56d) or (57c)
D_T	empirical constant defined in equation (54)
I_0	zeroth-order modified Bessel function of the first kind
K^*	permeability of the variable porosity packed bed
K^*_∞	permeability at the core of the packed bed
K	dimensionless permeability
K_0	zeroth-order modified Bessel function of the first kind
k_d^*	stagnant thermal conductivity of the saturated packed bed
k_e^*	effective thermal conductivity
k_f^*	thermal conductivity of the fluid
k_T^*	thermal dispersion coefficient
l	mixing length for transverse thermal dispersion
n	exponent defined in equation (55)
N_1	constant defined in equation (1)
N_2	constant in equation (3)
Nu_i	Nusselt number based on the inner cylinder defined in equation (59)
p^*	pressure
Pe	Péclet number
Pr	Prandtl number
q_{w_i}	heat flux at the wall of the inner cylinder
Re_p	Reynolds number based on particle diameter
T^*	temperature
T_o^*	temperature of the outer cylinder
T_i^*	temperature of the inner cylinder
$\hat{U}$	dimensionless inner velocity defined in equations (24b) and (38b)
$\hat{U}_0$	first-order inner velocity
u	dimensionless outer velocity
u^*	velocity in z^*-direction
u_0	first-order outer velocity
u_m^*	mean velocity defined in equation (10)
v^*	velocity in r^*-direction
z^*	coordinate along the axis of the annular bed
$\hat{R}$	dimensionless inner variable defined in equations (24a) and (38a)
r	dimensionless radial coordinate
$\hat{r}$	dimensionless outer variable defined in equations (17) and (32)
r^*	radial coordinate
r_i^*	radius of the inner cylinder
r_o^*	radius of the outer cylinder.

Greek symbols

α	dimensionless pressure drop parameter
β	empirical constant in the mixing length theory
γ	dimensionless parameter defined in equation (11)
ε	perturbation parameter defined in equation (19)
μ	viscosity of fluid
ν	kinematic viscosity of fluid
σ	dimensionless parameter defined in equation (12)
ω	dimensionless constant defined in equation (55)
ϕ^*	porosity of the packed bed.

Subscripts

w	wall condition
∞	condition away from the wall
i	quantity associated with the inner cylinder
o	quantity associated with the outer cylinder.

teristics. Closed form solutions for the temperature distribution and the Nusselt number are obtained based on three velocity models, i.e. Brinkman's model with variable and constant permeability as well as the plug flow model. Computations were carried out corresponding to the experiments conducted by Yagi and Kunii [12] for forced convection of air ($Pr = 0.7$) in an annular bed filled with glass beads. The fact that the heat transfer characteristics predicted in the present paper are in good agreement with experimental data reaffirms the validity of the mixing length concept and the Prandtl number dependence of the thermal dispersion coefficient. The present approach can easily be extended to the modeling of the transport processes in a catalytic bed.

VELOCITY DISTRIBUTION IN AN ANNULAR PACKED COLUMN

Measurements show that the porosity of a packed-sphere bed increases from a value of $0.36 \sim 0.4$ in the bulk of the bed to $0.8 \sim 1.0$ at the wall [13, 14]. The variation of the porosity takes the form of a damped oscillatory function with the oscillations damped out at about 4–5 sphere diameters from the wall. As shown in the previous papers [10, 15], the variation

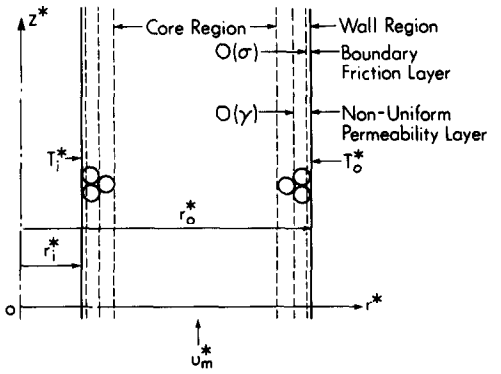

FIG. 1. Coordinate system.

of the porosity can be approximated by an exponential function. Thus, for a packed bed inside an annular with outer and inner radii r_o^* and r_i^* (see Fig. 1), the porosity can be approximated as

$$\phi^* = \phi_\infty^*\{1+C_1\exp[-N_1(r_o^*-r^*)/d_p]\},$$
$$(r_o^*-r_i^*)/2 \leqslant r^* \leqslant r_o^* \quad (1a)$$

$$\phi^* = \phi_\infty^*\{1+C_1\exp[-N_1(r^*-r_i^*)/d_p]\},$$
$$r_i^* \leqslant r^* \leqslant (r_o^*-r_i^*)/2 \quad (1b)$$

where ϕ_∞^* is the porosity at the bulk of the packed bed, d_p is the diameter of the particle and r^* is the radial coordinate. The constants ϕ_∞^*, C_1 and N_1 chosen in previous papers [10, 15] are $\phi_\infty^* = 0.4$, $C_1 = 1$ and $N_1 = 2$.

Since the permeability of a packed bed as a function of radius cannot be measured directly, its functional relationship can be inferred from equation (1) together with the following equation

$$K^* = d_p^2\phi^{*3}/A(1-\phi^*)^2 \quad (2)$$

where K^* is the permeability and $A = 150$ is an empirical constant [16]. For the purpose of obtaining an analytical solution for the flow field, the implicit relation between K^* and r^* as given by equations (1) and (2) can be approximated by an exponential function [10]

$$K^* = K_\infty^*\{1+C_2\exp[-N_2(r_o^*-r^*)/d_p]\},$$
$$(r_o^*-r_i^*)/2 \leqslant r^* \leqslant r_o^* \quad (3a)$$

$$K^* = K_\infty^*\{1+C_2\exp[-N_2(r^*-r_i^*)/d_p]\},$$
$$r_i^* \leqslant r^* \leqslant (r_o^*-r_i^*)/2 \quad (3b)$$

where K_∞^* is the permeability at the bulk of the packed bed which is given by

$$K_\infty^* = d_p^2\phi_\infty^{*3}/A(1-\phi_\infty^*)^2 = 1.185\times10^{-3}d_p^2$$

if $\phi_\infty^* = 0.4$ and $A = 150$. The constants C_2 and N_2 were obtained by matching equations (3) with the exact implicit function given by (1) and (2). This procedure was used in a previous paper [10] to obtain $C_2 = 20$ and $N_2 = 4$.

The governing equations based on the Brinkman model [17] for the velocity distribution of a fully-developed flow in a cylindrical packed bed are

$$\frac{\partial u^*}{\partial z^*} = 0, \quad v^* = 0 \quad (4a, b)$$

$$\frac{\mu u^*}{K^*} = -\frac{\partial p^*}{\partial z^*} + \frac{\mu}{r^*\phi^*}\frac{\partial}{\partial r^*}\left[r^*\frac{\partial u^*}{\partial r^*}\right] \quad (5)$$

$$\frac{\partial p^*}{\partial r^*} = 0 \quad (6)$$

where u^* and v^* are the velocities in the axial (z^*) and radial (r^*) directions, p^* is the pressure, and μ is the viscosity of the fluid. In equation (5) it is assumed that $\partial p^*/\partial z^*$ is constant, and that the inertia effect is neglected as a first approximation. In equations (4)–(6), we have implicitly assumed that $d_p \ll r_i^*$ so that the porous medium can be considered as a continuum.

The boundary conditions for the velocity are

$$r^* = r_i^*, \quad u^* = 0 \quad (7)$$

$$r^* = r_o^*, \quad u^* = 0. \quad (8)$$

Equations (1)–(8) are the governing equations and boundary conditions for the velocity distribution in a fully-developed flow in an annular packed bed with wall effects.

We now introduce the following dimensionless variables

$$u = u^*/u_m^*, \quad r = r^*/r_i^* \quad \text{and} \quad K = K^*/K_\infty^* \quad (9)$$

where u_m^* is the average velocity defined as

$$u_m^* = \frac{2}{(r_o^{*2}-r_i^{*2})}\int_{r_i^*}^{r_o^*} u^* r^*\,\mathrm{d}r^*. \quad (10)$$

Equations (3)–(6) and (10) in terms of these dimensionless variables are

$$K = 1+C_2\exp[-N_2(r-1)/\gamma],$$
$$\text{for } 1 \leqslant r \leqslant (r_o-1)/2 \quad (11a)$$

$$K = 1+C_2\exp[-N_2(r_o-r)/\gamma],$$
$$\text{for } (r_o-1)/2 \leqslant r \leqslant r_o \quad (11b)$$

$$\frac{u}{K} = \alpha + \frac{\sigma^2}{\phi r}\frac{\mathrm{d}}{\mathrm{d}r}\left(r\frac{\mathrm{d}u}{\mathrm{d}r}\right) \quad (12)$$

and

$$\int_1^{r_o} ur\,\mathrm{d}r = \frac{r_o^2-1}{2} \quad (13)$$

where

$$\alpha = -\frac{K_\infty^*}{\mu u_m^*}\frac{\mathrm{d}p^*}{\mathrm{d}z^*}, \quad r_o = r_o^*/r_i^*, \quad \gamma = d_p/r_i^*,$$

$$\sigma = \sqrt{\frac{K_\infty^*}{\phi_\infty^*}}\left(\frac{1}{r_i^*}\right) = \frac{\phi_\infty^*\gamma}{(1-\phi_\infty^*)\sqrt{A}} = 5.44\times10^{-2}\gamma$$

(if $\phi_\infty^* = 0.4$ and $A = 150$). Since $\sqrt{K_\infty^*/\phi_\infty^*} \ll d_p \ll r_i^*$, it follows that

$$\sigma \ll \gamma \ll 1. \tag{14}$$

Thus, the present problem contains two small parameters σ and γ. Equation (11) shows that the thickness of the non-uniform permeability layer is of $O(\gamma)$ while equation (12) shows that the thickness of the boundary friction layer is of $O(\sigma)$. The thickness of these layers is sketched in Fig. 1.

Equations (11)–(12) are to be solved subject to the boundary conditions

$$r = 1, \quad u = 0 \tag{15}$$

$$r = r_o, \quad u = 0. \tag{16}$$

We now obtain an analytical solution for equations (11)–(13) subject to boundary conditions (15) and (16) by the method of matched asymptotic expansions under the condition specified by equation (14).

FLOW FIELD NEAR THE INNER CYLINDER

To investigate the flow field near the inner wall at $r = 1$, the following new independent variable will be introduced:

$$\hat{r} = (r-1)/\gamma. \tag{17}$$

Equations (11a) and (12) in terms of the new variable are

$$K = 1 + C_2 e^{-N_2 \hat{r}} \tag{18}$$

$$\frac{u}{K} = \alpha + \frac{\varepsilon^2}{(1+\gamma\hat{r})\phi} \frac{d}{d\hat{r}}\left[(1+\gamma\hat{r})\frac{du}{d\hat{r}}\right] \tag{19}$$

where

$$\varepsilon = \frac{\sigma}{\gamma} = \frac{\phi_\infty^*}{(1-\phi_\infty^*)\sqrt{A}} = 5.44 \times 10^{-2} \ll 1.$$

Equations (18) and (19) are to be solved subject to the boundary conditions

$$\hat{r} = 0: \quad u = 0 \tag{20}$$

$$\hat{r} \to \infty: \quad u \text{ is finite.} \tag{21}$$

Non-uniform permeability layer near the inner cylinder

We now attempt to solve equations (18)–(21) by the method of matched asymptotic expansions. To this end, the dependent variable will be expanded in the following form

$$u = u_o + \varepsilon u_1 + O(\varepsilon^2) \tag{22}$$

Substituting equation (22) into (19) yields

$$u_o = \alpha K = \alpha[1 + C_2 e^{-N_2(r-1)/\gamma}] \tag{23}$$

which satisfies boundary condition (21) automatically.

Boundary friction layer near the inner cylinder

To investigate the boundary friction layer near the inner wall at $r = 1$, the following new independent variables will now be defined

$$\hat{R} = (r-1)/\sigma, \qquad \hat{U} = u. \tag{24a, b}$$

Substituting equation (24) into (11a) and (12) yields

$$K = 1 + C_2 e^{-\varepsilon N_2 \hat{R}}, \quad \phi = 1 + C_1 e^{-\varepsilon N_2 \hat{R}} \tag{25a, b}$$

$$\frac{\hat{U}}{K} = \alpha + \frac{1}{(1+\sigma\hat{R})\phi} \frac{d}{d\hat{R}}\left[(1+\sigma\hat{R})\frac{d\hat{U}}{d\hat{R}}\right] \tag{26}$$

which are to be solved subject to the boundary conditions

$$\hat{R} = 0: \quad \hat{U} = 0 \tag{27a}$$

$$\hat{R} \to \infty: \hat{U} \text{ must match with the solution for the non-uniform permeability layer.} \tag{27b}$$

To solve equations (25)–(27), U and K are expanded in the following form

$$\hat{U} = \hat{U}_o + \varepsilon \hat{U}_1 + O(\varepsilon^2) \tag{28a}$$

$$K = 1 + C_2 - \varepsilon C_2 N_2 \hat{R} + O(\varepsilon^2) \tag{28b}$$

$$\phi = 1 + C_1 - \varepsilon C_1 N_1 \hat{R} + O(\varepsilon^2). \tag{28c}$$

Substituting equations (28) into equations (25)–(27) yields the following first-order problem

$$\frac{\hat{U}_o}{1+C_2} = \alpha + \frac{1}{(1+\sigma\hat{R})C} \frac{d}{d\hat{R}}\left[(1+\sigma\hat{R})\frac{d\hat{U}_o}{d\hat{R}}\right] \tag{29}$$

where $C = 1 + C_1$. Equation (29) is to be solved subject to the boundary conditions

$$\hat{R} = 0: \quad \hat{U}_o = 0 \tag{30}$$

and as $\hat{R} \to \infty$, $\hat{U}_o$ must match with the solution of the non-uniform permeability layer.

It can be shown that the solution to equation (29) subject to boundary condition (30) is

$$\hat{U}_o = \alpha(1+C_2)\left\{1 - \frac{K_0[r\sqrt{C}/(\sigma\sqrt{1+C_2})]}{K_0[\sqrt{C}/(\sigma\sqrt{1+C_2})]}\right\} \tag{31}$$

where K_0 is the zeroth-order modified Bessel function of the second kind. Note that equation (31) matches with (23) under the limits of $\hat{R} \to \infty$ and $\hat{r} \to 0$.

FLOW FIELD NEAR THE OUTER CYLINDER

To investigate the flow field near the outer cylinder at $r = r_o$, the following new independent variable will now be introduced

$$\hat{r} = (r_o - r)/\gamma. \tag{32}$$

Equations (11b) and (12) in terms of the new variable are

$$K = 1 + C_2 e^{-N_2 \hat{r}}, \quad \phi = 1 + C_1 e^{-N_2 \hat{r}} \tag{33a, b}$$

$$\frac{u}{K} = \alpha + \frac{\varepsilon^2}{(r_o - \gamma\hat{r})\phi} \frac{d}{d\hat{r}}\left[(r_o - \gamma\hat{r})\frac{du}{d\hat{r}}\right] \tag{34}$$

which are to be solved subject to the conditions

$$\hat{r} = 0: \quad u = 0 \tag{35}$$

$$\hat{r} \to \infty: \quad u \text{ is finite.} \tag{36}$$

Non-uniform permeability layer near the outer cylinder

It can be shown that to the first order, the solution of the non-uniform permeability layer near the outer cylinder is

$$u_o = \alpha K = \alpha[1 + C_2 e^{-N_2(r_o - r)/\gamma}] \tag{37}$$

which satisfies boundary condition (36) automatically.

Boundary friction layer near the outer cylinder

To investigate the boundary friction layer near the outer cylinder (at r_o), the following variables will now be used

$$\hat{R} = \frac{r_o - r}{\sigma}, \quad \hat{U} = u. \tag{38a, b}$$

Substituting equations (38) into (11b) and (12) yields

$$K = 1 + C_2 e^{-\varepsilon N_2 \hat{R}} \tag{39}$$

$$\frac{\hat{U}}{K} = \alpha + \frac{1}{(r_o - \sigma\hat{R})C} \frac{d}{d\hat{R}}\left[(r_o - \sigma\hat{R})\frac{d\hat{U}}{d\hat{R}}\right] \tag{40}$$

which are to be solved subject to the boundary conditions (30). If $\hat{U}$ and K are expanded in the form of equation (28), the first-order problem becomes

$$\frac{\hat{U}_o}{1 + C_2} = \alpha + \frac{1}{(r_o - \sigma\hat{R})C} \frac{d}{d\hat{R}}\left[(r_o - \sigma\hat{R})\frac{d\hat{U}_o}{d\hat{R}}\right] \tag{41}$$

subject to the boundary conditions (30). It can be shown that the solution is

$$\hat{U}_o = \alpha(1 + C_2)\left\{1 - \frac{I_0[r\sqrt{C}/(\sigma\sqrt{1 + C_2})]}{I_0[r_o\sqrt{C}/(\sigma\sqrt{1 + C_2})]}\right\} \tag{42}$$

where I_0 is the zeroth-order modified Bessel function of the first kind. Again, equation (42) matches with (37) when $\hat{R} \to \infty$ and $\hat{r} \to 0$.

Uniformly valid solutions

A uniformly valid solution to the first-order can be constructed from equations (23), (31), (37) and (42) to give

$$u = \alpha\left\{1 + C_2[e^{-N_2(r-1)/\gamma} + e^{-N_2(r_o - r)/\gamma}] - (1 + C_2)\left[\frac{K_0[r\sqrt{C}/(\sigma\sqrt{1 + C_2})]}{K_0[\sqrt{C}/(\sigma\sqrt{1 + C_2})]} + \frac{I_0[r\sqrt{C}/(\sigma\sqrt{1 + C_2})]}{I_0[r_o\sqrt{C}/(\sigma\sqrt{1 + C_2})]}\right]\right\} + O(\varepsilon). \tag{43}$$

If modified Bessel functions are expanded asymptotically ($\sigma \to 0$), the above equation becomes

$$u = \alpha\left\{1 + C_2[e^{-N_2(r-1)/\gamma} + e^{-N_2(r_o - r)/\gamma}] - \frac{(1 + C_2)}{\sqrt{r}}\left(\exp\left[-\frac{(r-1)\sqrt{C}}{\sigma\sqrt{1 + C_2}}\right] + \sqrt{r_o}\exp\left[-\frac{(r_o - r)\sqrt{C}}{\sigma\sqrt{1 + C_2}}\right]\right)\right\} + O(\varepsilon) \tag{44}$$

where α can be determined by substituting equation (44) into (13) to yield

$$\alpha = \left(\frac{r_o^2 - 1}{2}\right)\Big/\left\{\frac{r_o^2 - 1}{2} + \frac{C_2\gamma}{N_2}(r_o + 1) \times [1 - e^{-N_2(r_o - 1)/\gamma}] - (1 + C_2)\left(\int_1^{r_o}\sqrt{r} \times \exp\left[-\frac{(r-1)\sqrt{C}}{\sigma\sqrt{1 + C_2}}\right]dr + \sqrt{r_o}\int_1^{r_o}\sqrt{r} \times \exp\left[-\frac{(r_o - r)\sqrt{C}}{\sigma\sqrt{1 + C_2}}\right]dr\right)\right\} + O(\varepsilon). \tag{45}$$

If the permeability is assumed to be constant (i.e. the Brinkman model with constant permeability), equations (44) and (45) with $C_2 = \gamma = 0$ give

$$u = \alpha\left\{1 - \frac{1}{\sqrt{r}}[e^{-(r-1)\sqrt{C}/\sigma} + \sqrt{r_o}\, e^{-(r_o - r)\sqrt{C}/\sigma}]\right\} \tag{46}$$

and

$$\alpha = \left(\frac{r_o^2 - 1}{2}\right)\Big/\left\{\frac{r_o^2 - 1}{2} - \left[\int_1^{r_o}\sqrt{r}\, e^{-(r-1)\sqrt{C}/\sigma}\, dr + \sqrt{r_o}\int_1^{r_o}\sqrt{r}\, e^{-(r_o - r)\sqrt{C}/\sigma}\, dr\right]\right\}. \tag{47}$$

The plug flow model is equivalent to setting $\sigma = 0$ in equations (46) and (47) to give

$$u = \alpha = 1. \tag{48}$$

NUMERICAL RESULTS FOR VELOCITY DISTRIBUTION

Equations (43) and (44) show that the velocity profile for a variable permeability annular bed depends on the values of C_2, N_2, γ and r_o. With

$$C_2 = 20, \; N_2 = 4, \; \sigma = \sqrt{\frac{K_\infty^*}{\phi_\infty^*}}\Big/ r_i^* = 5.44 \times 10^{-2}\gamma$$

the velocity distribution depends only on γ and r_o. Figure 2 shows the effect of γ on the axial velocity distribution in an annular packed bed with inner and outer radii of 0.011 m and 0.035 m (i.e. $r_o = 3.18$), which was the packed bed used by Yagi and Kunii [12]. The three values of γ correspond to the three

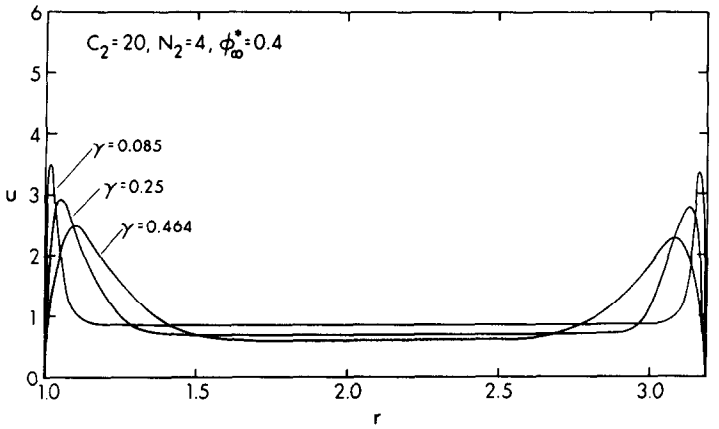

FIG. 2. Wall channeling effect on axial velocity.

different sizes of the particle diameters used in Yagi and Kunii's experiments (see Table 1). It is shown from Fig. 2 that the velocity overshoot occurs in the variable permeability bed near the inner and outer cylinders. The magnitude of the velocity overshoot increases as γ is decreased. The velocity overshoot is slightly higher near the inner cylinder (at $r = 1$) than that near the outer cylinder (at $r = r_o$). The maximum velocity occurs at about 1/4 particle diameter away from the inner cylinder, and about 1/3 particle diameter away from the outer cylinder. The shape of the velocity profile presented in Fig. 2 is in qualitative agreement with the variational solution obtained by Vortmeyer and Schuster [15] for small and moderate values of Re_p ($Re_p < 100$).

HEAT TRANSFER CHARACTERISTICS IN THE ANNULAR PACKED COLUMN

We now consider the heat transfer characteristics of the fully-developed forced convective flow in the annular packed column at temperatures T_i^* and T_o^*. As shown in Fig. 1, the thermal boundary conditions for the problem are

$$r^* = r_i^*, \quad T^* = T_i^* \tag{49a}$$

$$r^* = r_o^*, \quad T^* = T_o^*. \tag{49b}$$

For an annular packed column that is heated and cooled circumferentially, the thermally fully-developed flow can be defined as

$$\frac{\partial T^*}{\partial z^*} = 0 \tag{50}$$

With the aid of equations (4b) and (50), the energy equation for the forced convective flow is

$$\frac{\mathrm{d}}{\mathrm{d}r^*}\left(k_e^* r^* \frac{\mathrm{d}T^*}{\mathrm{d}r^*}\right) = 0 \tag{51}$$

where k_e^* is the effective radial thermal conducivity of the packed bed which is a superposition of the stagnant thermal conductivity (k_d^*) and the radial dispersion coefficient (k_T^*), i.e.

$$k_e^* = k_d^* + k_T^*. \tag{52}$$

The value of k_d^* can be computed from the following

Table 1. Experiments conducted by Yagi and Kunii [12]

Run No.	d_p (m)	Re_p	T_o^* (°C)	T_i^* (°C)	h_{w_i} (kcal m^{-2} h^{-1} °C^{-1})	Δt_1 (°C)	q_{w_i} (W m^{-2})	γ	Materials
A-6	0.00057	7.8	100	8	170	9	1776	0.051	Glass beads and air
A-11	0.00057	17.6	100	8	185	8	1718	0.051	Glass beads and air
A-17	0.00057	32.4	100	8	170	9	1776	0.051	Glass beads and air
B-6	0.00094	14.3	100	16	70.0	19	1544	0.085	Glass beads and air
B-12	0.00094	32.2	100	17	95.5	14.5	1607	0.085	Glass beads and air
B-19	0.00094	75.3	100	16	142.0	12.5	2061	0.085	Glass beads and air
C-4	0.00275	74.0	100	19	82.7	19.0	1824	0.25	Glass beads and air
C-9	0.00275	131.0	100	19	85.5	19.0	1886	0.25	Glass beads and air
C-20	0.00275	266.0	100	15	107.0	21.0	2608	0.25	Glass beads and air
C-26	0.00275	372.0	100	15	145.0	21.5	3619	0.25	Glass beads and air
D-9	0.0051	178.0	100	13.5	75.0	24.0	2089	0.464	Glass beads and air
D-13	0.0051	236.0	100	13.5	85.9	23.0	2293	0.464	Glass beads and air
D-19	0.0051	332.0	100	13.5	99.5	26.0	3003	0.464	Glass beads and air

semi-analytical equation given by Zehner and Schluender [19]

$$\frac{k_d^*}{k_f^*} = [1-\sqrt{1-\phi^*}] + \frac{2\sqrt{1-\phi^*}}{1-\lambda B} \times \left[\frac{(1-\lambda)B}{(1-\lambda B)^2}\ln\frac{1}{\lambda B} - \frac{B+1}{2} - \frac{B-1}{1-\lambda B}\right] \quad (53)$$

where $B = 1.25[(1-\phi^*)/\phi^*]^{10/9}$ and $\lambda = k_f^*/k_s^*$ with k_f^* and k_s^* denoting the thermal conductivity of the fluid and the solid particle respectively. Equation (53) shows that the stagnant thermal conductivity is a function of position for a variable porosity bed.

As proposed by Cheng and Vortmeyer [10], we now assume that the radial thermal dispersion coefficient k_T^* is of the form

$$k_T^*/k_f^* = D_T\, Pe\, ul \quad (54)$$

where $Pe = Pr\, Re_p$ with Pr denoting the Prandtl number of the fluid, and $Re_p = u_m^* d_p/\nu$ is the Reynolds number based on the mean velocity and the particle diameter, and l is the mixing length for radial thermal dispersion which is given by

$$l = \begin{cases} \left(\dfrac{r^*-r_i^*}{\beta d_p}\right)^n & \text{for the inner wall region } (r_i^* \leqslant r^* \leqslant r_i^*+\beta d_p) \\ 1 & \text{for the core region } (r_i^*+\beta d_p \leqslant r^* \leqslant r_o^*-\beta d_p) \\ \left(\dfrac{r_o^*-r^*}{\beta d_p}\right)^n & \text{for the outer wall region } (r_o^*-\beta d_p \leqslant r^* \leqslant r_o^*) \end{cases}$$

or

$$l = \begin{cases} \left(\dfrac{r-1}{\omega}\right)^n & \text{for } 1 \leqslant r \leqslant 1+\omega \\ 1 & \text{for } 1+\omega \leqslant r \leqslant r_o-\omega \\ \left(\dfrac{r_o-r}{\omega}\right)^n & \text{for } r_o-\omega \leqslant r < r_o \end{cases} \quad (55)$$

where $\omega = \beta d_p/r_i^*$. Cheng and Vortmeyer [10] found that with $\beta = 0$ (i.e. wall effects on transverse thermal dispersion is unimportant), the large temperature drops observed in Schroeder *et al.*'s data [11] cannot be reproduced with the theory. They found that the values of $n = 1$, $D_T = 0.2 \sim 0.25$ and $\beta = 2 \sim 2.5$ match the theory with Schroeder *et al.*'s data well. Equations (55) show that the mixing length in the wall regions varies linearly with the distance from the wall, and that the effect of a bounding wall on the radial thermal dispersion vanishes at a distance of $2 \sim 2.5$ particle diameters away from the wall.

Solution of the radial temperature distribution

Equations (51)–(55) with u given by equation (43), (46) or (48) subject to boundary conditions (49) can be obtained by a direct integration. Since the expression for the mixing length given by equation (55) depends on location, the solution of temperature distribution depends on the region under consideration. Moreover, the solution depends on whether the effect of the wall on the radial thermal dispersion is felt over part of the bed or the entire bed, i.e. $(r_o^*-r_i^*)/2 > \beta d_p$ or $(r_o^*-r_i^*)/2 \leqslant \beta d_p$.

(i) For the case of $(r_o^*-r_i^*)/2 > \beta d_p$ or $r_o > 2\omega+1$, the temperature is given by

$$T^*(r) = T_i^* + D\int_1^r \frac{dr}{r\{k_d^*+D_T k_f^*\, Pr\, Re_p u[(r-1)/\omega]^n\}}$$

for the inner wall region, $1 \leqslant r \leqslant 1+\omega$ (56a)

$$T^*(r) = T^*(1+\omega) + D\int_{1+\omega}^r \frac{dr}{r(k_d^*+D_T k_f^*\, Pr\, Re_p u)}$$

for the core region, $1+\omega \leqslant r \leqslant r_o-\omega$ (56b)

$$T^*(r) = T^*(r_o-\omega) + D\int_{r_o-\omega}^r \frac{dr}{r\{k_d^*+D_T k_f^*\, Pr\, Re_p u[(r_o-r)/\omega]^n\}}$$

for the outer wall region, $r_o-\omega \leqslant r \leqslant r_o$ (56c)

where

$$D = (T_o^*-T_i^*)\Big/\left\{\int_1^{1+\omega} \frac{dr}{r\{k_d^*+D_T k_f^*\, Pr\, Re_p u[(r-1)/\omega]^n\}} + \int_{1+\omega}^{r_o-\omega} \frac{dr}{r(k_d^*+D_T k_f^*\, Pr\, Re_p u)} + \int_{(r_o-\omega)}^{r_o} \frac{dr}{r\{k_d^*+D_T k_f^*\, Pr\, Re_p u[(r_o-r)/\omega]^n\}}\right\}. \quad (56d)$$

(ii) For the case of $(r_o^*-r_i^*)/2 \leqslant \beta d_p$, or $r_o \leqslant 2\omega+1$, the wall effect is felt over the entire bed. In this case, the temperature distribution is given by

$$T^*(r) = T_i^* + D\int_1^r \frac{dr}{r\{k_d^*+D_T k_f^*\, Pr\, Re_p u[(r-1)/\omega]^n\}}$$

for the inner wall region, $1 \leqslant r \leqslant (r_o-1)/2$ (57a)

$$T^*(r) = T^*\left(\frac{r_o-1}{2}\right) + D\int_{(r_o-1)/2}^r \frac{dr}{r\{k_d^*+D_T k_f^*\, Pr\, Re_p u[(r_o-r)/\omega]^n\}}$$

for the outer wall region, $(r_o-1)/2 \leqslant r \leqslant r_o$ (57b)

where

$$D = (T_o^*-T_i^*)\Big/\left\{\int_1^{(r_o-1)/2} \frac{dr}{r\{k_d^*+D_T k_f^*\, Pr\, Re_p u[(r-1)/\omega]^n\}} + \int_{(r_o-1)/2}^r \frac{dr}{r\{k_d^*+D_T k_f^*\, Pr\, Re_p u[(r_o-r)/\omega]^n\}}\right\}. \quad (57c)$$

The surface heat flux from the inner cylinder is

$$q_{w_i} = -\left(k_e^* \frac{dT^*}{dr^*}\right)_{r^*=r_i^*} = -\frac{D}{r_i^*} \tag{58}$$

which can be rewritten in dimensionless form as

$$Nu_i = \frac{q_{w_i} r_i^*}{k_f^*(T_o^* - T_i^*)} = -\frac{D}{k_f^*(T_o^* - T_i^*)} \tag{59}$$

where Nu_i is the Nusselt number based on the radius of the inner cylinder.

NUMERICAL RESULTS FOR HEAT TRANSFER CHARACTERISTICS

Equations (56)–(59) show that the heat transfer characteristics in an annular packed bed depend on the values of n, β, D_T, d_p, r_o, k_s^*, k_f^*, T_i^*, T_o^*, Pr, Re_p, C_1 and N_1. They also depend on the values of C_2 and N_2 implicitly through their dependence on the velocity profile. Computations for the heat transfer characteristics were carried out for the 13 experimental runs conducted by Yagi and Kunii [12]. These experiments were carried out with air ($Pr = 0.7$ and $k_f^* = 0.027$ W m^{-1} K^{-1}) flowing through an annular packed bed comprised of glass beads ($k_s^* = 1.05$ W m^{-1} K^{-1}). Other experimental conditions (d_p, Re_p, T_i^* and T_o^*) together with the experimentally determined wall heat transfer coefficient from the inner cylinder (h_{w1}) and temperature difference (Δt_1) are listed in Table 1. Also listed in the table are the experimentally determined values of surface heat flux from the inner cylinder q_{wi}, which were computed according to

$$q_{wi} = h_{w1} \Delta t_1. \tag{60}$$

Other experiments performed by Yagi and Kunii [12] with $\gamma > 0.4$ are not listed in Table 1.

Computations for the heat transfer characteristics were carried out based on the three velocity models [i.e. Brinkman's model with variable and constant permeability as well as the plug flow model as given by equations (44), (46) and (48)]. It is relevant to mention that the radial variation of the stagnant thermal conductivity (due to porosity variation) must be taken into consideration even though the constant permeability assumption is used in the computations of the velocity profiles [i.e. equations (46) and (48)]. It was found that if the values of $n = 1$, $\beta = 2$, $D_T = 0.2$, $C_1 = 1.4$ and $N_1 = 2$ are used in the theory, the predicted heat transfer characteristics based on the three velocity models match with experimental data.

Of the 13 experimental runs listed in Table 1, Yagi and Kunii [12] chose to present the temperature distribution data only for one case (C-9). Since the experimental conditions for other temperature data presented in Yagi and Kunii's paper are not reported explicitly, simulations of these temperature data cannot be performed. A detailed comparison of temperature distribution between experiments and theory (based on the three velocity models) can therefore only be made for the case of C-9, which is displayed in Fig. 3b. It is shown that the predicted temperature distribution based on the Brinkman model with a variable permeability (shown as a solid line in the figure) predicts a smaller temperature drop near the walls than that of the other two velocity models (shown as dashed lines), and that the solid line agrees the best with experimental data.

The predicted temperature distribution for the case of B-12 ($Re_p = 32.2$ and $\gamma = 0.085$) is presented in Fig. 3a. At a low Reynolds number of 32.2 and a small value of γ, the predicted temperature distributions based on the Brinkman model with a constant per-

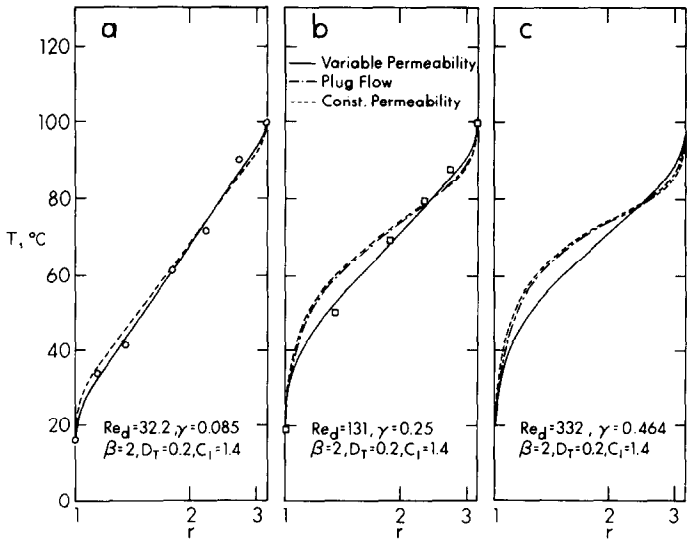

FIG. 3. Comparison of predicted and experimentally determined temperature profiles in an annular packed column.

meability and the plug flow model are indiscernible in the graph. The temperature data presented in Fig. 3a is actually for case B-14 with $Re_p = 40.6$ which is slightly higher than the simulated data with $Re_p = 32.2$. Again, it is shown that the predicted temperature distribution based on the Brinkman model with a variable permeability agrees the best with experimental data.

The predicted temperature distributions based on the three velocity models for the case of D-19 ($Re_p = 332$ and $\gamma = 0.4$) are presented in Fig. 3c. It is shown that at a high value of $\gamma = 0.4$, the predicted temperature distribution near the cooled inner surface based on the plug flow model or the Brinkman model with constant permeability is substantially higher than that of the Brinkman model with a variable permeability.

A comparison of the predicted and experimentally determined Nusselt number based on the inner cylinder of the annular packed bed as a function of the Reynolds number at four values of γ is displayed in Fig. 4. The predicted Nusselt numbers based on three velocity models, are shown to be in good agreement with experimental data. At a low value of γ ($\gamma = 0.051$ for example), the predicted Nusselt numbers based on the three velocity models are indiscernible in the graph. At higher values of γ and Re_p ($\gamma = 0.464$ and $Re_p > 100$), the Nusselt number predicted by the plug flow model is higher than those of the Brinkman model with variable or constant permeability. Thus, the shape of the velocity profile has a relatively small effect on the Nusselt number at small and moderate values of Re_p ($Re_p < 100$). It is relevant to note that for a given value of γ, the slope of the Nu_i vs Re_p curve increases from zero as the value of Re_p is increased.

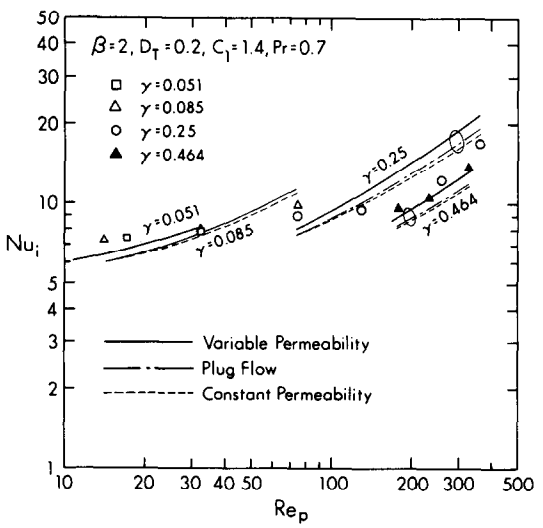

FIG. 4. Comparison of predicted and experimentally determined Nusselt number in an annular packed column.

CONCLUDING REMARKS

The mixing length theory, proposed by Cheng and Vortmeyer [10] for transverse thermal dispersion in a packed bed with a bounding wall, is applied to the problem of fully-developed, forced convective flow through an annular bed. With the values of $\beta = 2.0$ and $D_T = 0.2$ used in the mixing length theory, the predicted heat transfer characteristics based on the three velocity models are found in good agreement with experimental data. With these values the predicted temperature profiles based on the variable permeability model agree the best with experimental data. Presumably, if other values of β and D_T are used in the theory, a closer match between experimental data and theory based on the plug flow model and the Brinkman model with a constant permeability can be achieved. This has not been attempted in view of the approximate nature of the theory. The results of the present analysis, however, do reinforce the validity of the mixing length theory and the Prandtl number dependence of the radial thermal dispersion coefficient.

One of the assumptions made in the present analysis is that the inertia effect (i.e. the velocity square term in the momentum equation) is negligible. For high-speed forced convective flow in a packed bed where the nonlinear term in the momentum equation must be included, a closed form solution for the velocity distribution may not be possible and numerical solution is preferred. This aspect of the problem is presently under investigation.

Acknowledgement—This work was supported by NSF Grant No. C13T 83-12095.

REFERENCES

1. G. F. Froment, Analysis and design of fixed bed catalytic reactors, *Chem. Reaction Engng* **109,** 1–34 (1972).
2. C. H. Li and B. A. Finlayson, Heat transfer in packed beds—a re-evaluation, *Chem. Engng Sci.* **32,** 1055–1066 (1977).
3. R. E. Chao, R. A. Caban and M. M. Irizarry, Wall heat transfer to chemical reactors, *Can. J. Chem. Engng* **51,** 67–70 (1973).
4. W. R. Paterson and J. J. Carberry, Fixed bed catalytic reactor modelling, *Chem. Engng Sci.* **38,** 175–180 (1983).
5. J. J. Lerou and G. F. Froment, Velocity, temperature and conversion profiles in fixed bed catalytic reactors, *Chem. Engng Sci.* **32,** 853–861 (1977).
6. O. Kalthoff and D. Vortmeyer, Ignition/extinction phenomena in a wall cooled fixed bed reactor, *Chem. Engng Sci.* **35,** 1637–1643 (1980).
7. D. Vortmeyer and R. F. Winter, Improvements in reactor analysis incorporating porosity and velocity profiles, *Germ. chem. Engng* **7,** 19–25 (1984).
8. D. Arntz, K. Knapp, G. Prescher, G. Enig and H. Hofman, *ACS Symp. Ser.* **196,** 3 (1982).
9. M. Ahmed and R. W. Fahien, Tubular reactor design—I. Two-dimensional model, *Chem. Engng Sci.* **35,** 889–895 (1980).
10. P. Cheng and D. Vortmeyer, Transverse thermal dis-

persion and velocity profile in a packed bed with forced convective flow, *Chem. Engng Sci.* (in press).
11. K. J. Schroeder, V. Renz and K. Elegeti, *Forschungsberichte des Landes Nordrhein-Westfalen*, Nr. 3037 (1981).
12. S. Yagi and D. Kunii, Studies of heat transfer near wall surface in packed beds, *A.I.Ch.E. Jl* **6**, 97–104 (1960).
13. L. H. S. Roblee, R. M. Baird and J. W. Tiern, Radial porosity variations in packed beds, *A.I.Ch.E. Jl* **4**, 460–464 (1958).
14. R. F. Benenati and C. B. Brosilow, Void fraction distribution in beds of sphere, *A.I.Ch.E. Jl* **8**, 359–361 (1962).
15. D. Vortmeyer and J. Schuster, Evaluation of steady flow profiles in rectangular and circular packed beds by a variational method, *Chem. Engng Sci.* **38**, 1691–1699 (1983).
16. S. Ergun, Fluid flow through packed columns, *Chem. Engng Prog.* **48**, 89–94 (1952).
17. H. C. Brinkman, A calculation of the viscous force exerted by a flowing fluid on a dense swarm of particles, *Appl. scient. Res.* **A1**, 27 (1947).
18. K. Vafai, Convective flow and heat transfer in variable-porosity media, *J. Fluid Mech.* **147**, 233–259 (1984).
19. P. Zehner and E. U. Schluender, Waermeleitfahigkeit von Schuettungen bei massigen Temperaturen, *Chemie-Ingr-Tech.* **42**, 933–941 (1970).

ECOULEMENT DE CONVECTION FORCEE ETABLI A TRAVERS UN LIT FIXE DE SPHERES ANNULAIRE AVEC EFFET DE PAROI

Résumé—On analyse l'écoulement forcé convectif établi à travers un lit fixe de sphères entre deux cylindres concentriques maintenus à différentes températures. Les variations radiales de la porosité et de la perméabilité dans le lit près des parois, connues comme effets de paroi, sont approchées par des fonctions exponentielles. Le modèle de Brinkman avec perméabilité variable est utilisé. Une solution analytique basée sur la méthode des développements asymptotiques est obtenue pour la distribution de vitesse. On montre que des survitesses apparaissent près des cylindres, avec une importance légèrement plus grande près du cylindre intérieur. A cause de la variation non uniforme de porosité près des parois, la conductivité thermique fixe du lit varie aussi dans la direction radiale. Une théorie de longueur de mélange, proposée récemment par Cheng et Vortmeyer pour la dispersion thermique est utilisée pour obtenir la distribution radiale de température et le nombre de Nusselt du lit annulaire. Des calculs thermiques sont conduits sur trois modèles dynamiques, modèle de Brinkman avec perméabilité constante et variable et modèle d'écoulement piston. On trouve qu'avec la théorie de la longueur de mélange, les prédictions des caractéristiques thermiques basées sur les trois modèles de vitesse sont en bon accord avec les données expérimentales. Les profils de température calculés avec le modèle de Brinkman à perméabilité variable s'accordent mieux avec les mesures de température.

VOLL AUSGEBILDETE ERZWUNGENE KONVEKTIONSSTRÖMUNG DURCH EIN RINGFÖRMIGES KUGELSCHÜTTBETT MIT RANDEFFEKTEN

Zusammenfassung—Es wird eine Untersuchung für eine voll ausgebildete erzwungene Konvektionsströmung durch ein ringförmiges Kugelschüttbett zwischen zwei konzentrischen Zylindern unterschiedlicher Temperatur vorgestellt. Die Änderungen von Porosität und Permeabilität in radialer Richtung nahe der Wand, als Wandeffekte bekannt, werden durch Exponentialfunktionen angenähert. Als Impulsgleichung wird das Brinkman-Modell mit unterschiedlicher Permeabilität verwendet. Für die Geschwindigkeitsverteilung erhält man eine analytische Lösung, die auf der Methode der asymptotischen Anpassung basiert. Es zeigen sich Übergeschwindigkeiten in der Zone variabler Permeabilität in Wandnähe des inneren und äußeren Zylinders. Die Übergeschwindigkeit ist am inneren Zylinder mit dem kleineren Radius etwas höher. Wegen der ungleichmäßigen Porositätsänderung in Wandnähe ändert sich somit die Wärmeleitfähigkeit des Betts auch in radialer Richtung. Es wird eine kürzlich von Cheng und Vortmeyer vorgeschlagene Mischungslängentheorie für die thermische Querausbreitung verwendet, um die radiale Temperaturverteilung und die Nusselt-Zahl für das ringförmige Bett zu ermitteln. Mit drei Geschwindigkeitsmodellen (dem Brinkman-Modell mit variablen und konstanten Permeabilitäten und dem Pfropfenströmungsmodell), wurden Berechnungen der Wärmeübertragungscharakteristiken durchgeführt. Mit der Mischungslängentheorie ergab sich eine gute Übereinstimmung der theoretischen Vorhersagen der Wärmeübergangscharakteristiken, basierend auf den drei Geschwindigkeitsmodellen, mit den Experimenten. Die vorhergesagten Temperaturprofile, die mit dem Brinkman-Modell mit variabler Permeabilität ermittelt wurden, stimmen am besten mit den Temperaturmessungen überein.

ПОЛНОСТЬЮ РАЗВИТОЕ ВЫНУЖДЕННО-КОНВЕКТИВНОЕ ТЕЧЕНИЕ ЧЕРЕЗ КОЛЬЦЕВОЙ, ЗАПОЛНЕННЫЙ СФЕРИЧЕСКИМИ ЧАСТИЦАМИ СЛОЙ, С УЧЕТОМ ПРИСТЕННЫХ ЭФФЕКТОВ

Аннотация—Анализируется полностью развитое вынужденно-конвективное течение через заполненный сферическими частицами слой между концентрическими цилиндрами, имеющими разные температуры. Радиальные изменения порозности и проницаемости в слое вблизи стенок, известные как пристенные эффекты, аппроксимировались с помощью экспоненциальных функций. В качестве уравнения количества движения использовалась модель Бринкмана с изменяющейся проницаемостью. Получено аналитическое решение, основанное на методе сращиваемых асимптотических разложений, позволяющее рассчитывать поле скоростей в слое. Показано, что в слое с переменной проницаемостью вблизи внутреннего и наружного цилиндров скорость выше, чем в остальном объеме слоя. Величина этого превышения скорости несколько больше у внутреннего цилиндра с меньшим радиусом. Теплопроводность слоя также меняется в радиальном направлении из-за неоднородного изменения порозности около стенок. Теория длины пути смешения, предложенная Ченгом и фортмейером для поперечной тепловой дисперсии, используется для нахождения радиального распределения температур и числа Нуссельта кольцевого слоя. Характеристики теплопереноса рассчитаны на основе трехскоростных моделей, т.е. модели Бринкмана с переменными и постоянными проницаемостями и модели поршневого течения. Обнаружено, что при использовании теории пути длины смешения теоретические расчеты характеристик теплообмена, основанные на трехскоростных моделях, хорошо согласуются с имеющимися экспериментальными данными. Профили температур, рассчитанные по модели Бринкмана с изменяющейся проницаемостью, хорошо соответствуют данным температурных изменений.